DOI: 10.1002/ ((please add manuscript number))

Article type: Communication

Improved Domain Size and Purity Enables Efficient All-Small-Molecule Ternary Solar Cells

Hao Zhang, Xiaohui Wang, Liyan Yang, Shaoqing Zhang, Yun Zhang, Chang He, Wei Ma*, Jianhui Hou.**

H. Zhang, L. Yang, Dr. S. Zhang, Y. Zhang, Prof. C. He, Prof. J. Hou

State Key Laboratory of Polymer Physics and Chemistry

Beijing National Laboratory for Molecular Sciences

Institute of Chemistry

Chinese Academy of Sciences

Beijing 100190, P.R. China

E-mail: hjhzlz@iccas.ac.cn; hechang@iccas.ac.cn

H. Zhang, L. Yang, Y. Zhang, Prof. C. He, Prof. J. Hou

University of Chinese Academy of Sciences

Beijing 100049, P. R. China

X. Wang, Prof. W. Ma

State Key Laboratory for Mechanical Behavior of Materials

Xi'an Jiaotong University

Xi'an 710049, P.R. China

E-mail: msewma@mail.xjtu.edu.cn

Keywords: organic solar cells; non-fullerene; ternary; domain purity; small molecule

Abstract: An all-small-molecule ternary solar cell was achieved with a power conversion efficiency of 10.48% by incorporating $PC_{71}BM$ into a non-fullerene DRTB-T:IDIC binary system. The addition of $PC_{71}BM$ into DRTB-T:IDIC was found to modulate the film morphology by improving the domain purity and decreasing the domain size. This modulation facilitated the charge generation and suppressed charge recombination, as manifested by the significantly enhanced short-circuit current density and fill factor. The results correlated the domain characteristics with the device performance and offered new insight from the perspective of morphology modulation for constructing efficient ternary devices.

Organic solar cell (OSC) has garnered increasing attention since it has emerged as a promising low-cost solution for energy conversion. [1-4] Recently, with the advances in photovoltaic material design and device optimization, OSC performance has rapidly increased, leading to a breakthrough in the power conversion efficiency (PCE) of over 12%.[5-7] Nonetheless, due to their wide optical bandgap, OSC devices cannot utilize a large proportion of the incident photons, which impedes further enhancement of the PCE. Taking advantage of multiple components with complementary absorption spectra to harvest more solar radiation has been commonly accepted as a useful strategy to address

this restriction. For instance, tandem solar cells are a successful and well-developed example of this strategy.[5, 7-9] However, the sophisticated configurations of tandem OSCs, including the processing of the intermediate layer and the strict control of the film thickness, complicate the fabrication and weaken the reproducibility of their performance.[5, 7] Ternary OSCs that integrate multiple photovoltaic materials into one active layer are an effective alternative routine in overcoming these problems.[10-16] In addition to supplementing the absorption spectra, ternary devices also have other unique advantages. The added third components can improve the film morphology and/or align the energy level cascade.[15-19]

Nearly all ternary devices have been fabricated using polymer donor-based solar cells. The all-small-molecule solar cells have rarely been investigated, and their PCE still lag behind their polymeric counterparts. However, small molecules possess some remarkable merits, including a well-defined molecular structure, less batch-to-batch variance, easy purification and good solubility.[20-23] Nonetheless, unlike the conjugated polymer, small molecules have no long backbones to weave a continuous network skeleton. Meanwhile, small molecules with improved crystallinity tend to cause strong aggregation and large crystalline domains, which may deteriorate the photovoltaic process. When introducing a third component, the miscibility and interaction among the multiple components further add complexity to the morphology-tuning of ternary devices. Hence, understanding the evolution of film morphology and achieving the proper phase separation and domain characteristics are issues that must be addressed in constructing highly efficient all-small-molecule ternary devices but remain vague and unexplored.[24-28] On the other hand, in practice, if the synergistic effect on modulating morphology of the third component is well manipulated, a high PCE is anticipated.

Recently, non-fullerene acceptors (NFAs) have quickly progressed and obtained substantive achievements.[21, 29-35] Compared with fullerene derivative acceptors, the absorption spectrum, molecular orbital energy level and molecular arrangement can be well tuned due to their relatively easy chemical modification, which makes NFAs ideal for constructing ternary solar cells. Here, we incorporated fullerene acceptors, i.e., phenyl-C_{71}-butyric-acid-methyl ester ($PC_{71}BM$) into the NFA-based devices to fabricate all-small-molecule ternary OSCs. In addition, to vary the relative component content, we adopted solvent vapor annealing (SVA) [36] to optimize the device performance and finally realized a PCE of 10.48%. The film morphology study demonstrated that the presence of $PC_{71}BM$ limited the excessive growth of crystal structures and thus formed the appropriate phase separated scale. Moreover, more compact molecular stacking and purer domains were achieved, which increased the charge generation and suppressed the charge recombination. The synergistic effect of the complementing absorption spectra and modulating film morphology of the $PC_{71}BM$ enhanced the entire light harvesting spectrum and led to an efficient all-small-molecule OSC device.

Previously, we reported an efficient acceptor-donor-acceptor structured small molecule donor, DRTB-T, containing a ter-benzodithiophene core flanked with rhodanine groups.[21] This small molecule donor delivered a PCE beyond 9% when blended with a non-fullerene small molecule acceptor, namely, IDIC (depicted in **Figure 1a**).[21, 37] Like most small molecule solar cells, the devices showed moderate short-circuit current density (J_{SC}) due to the limited photo response range. As shown in **Figure 1b**, the donor and NFA have complementary absorption spectra with separate absorption peaks centered at *ca.* 535 nm and 700 nm, respectively. However, the absorption intensity was weak for shorter wavelengths. Hence, it is reasonable to include $PC_{71}BM$, with its

primary absorption region ranging from 300 to 500 nm, as the third component (A2) to assist photon harvesting and further boost the efficiency of the OSC devices. The absorption coefficients of the pristine film of DRTB-T, IDIC and $PC_{71}BM$ were 1.1×10^5, 1.8×10^5 and 1.0×10^5 cm^{-1}, respectively. The UV-Vis absorption spectrum of the ternary blend films containing $PC_{71}BM$ was significantly extended, as shown in **Figure 1b**. After annealing the film with tetrahydrofuran (THF) vapor for 10 min, the absorption edge of the ternary film exhibited a significant redshift of approximately 40 nm in the near-infrared region, which implied a strong aggregation of the acceptor after SVA. In addition to the absorption spectra, from the energy level diagram shown in **Figure 1c**, both the highest occupied molecular orbital (HOMO) and highest unoccupied molecular orbital (LUMO) of $PC_{71}BM$ is lower than those of the non-fullerene acceptor. This favors the formation of a cascade energy level alignment and facilitates charge transfer.

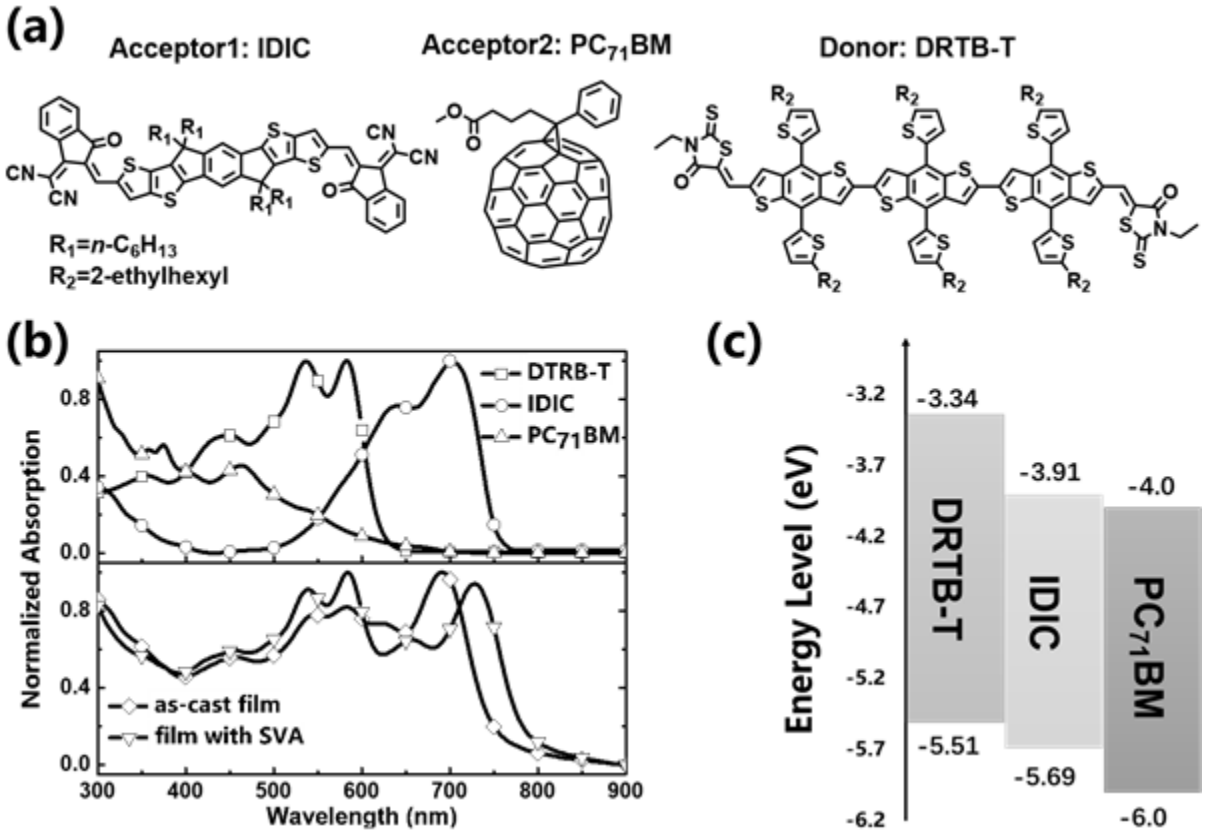

Figure 1. (a) Molecular structures of the donor and acceptors. (b) Absorption spectra of the neat donor, acceptors and ternary blend films. (c) Molecular energy level of the donor and acceptors.

The photovoltaic properties of the active layers were evaluated by fabricating OSC devices with an architecture of ITO/PEDOT:PSS/Active Layer/Mg/Al, where PEDOT:PSS was poly(3,4-ethylenedioxythiophene)-poly(styrene sulfonate) and was used as an anode buffer layer. The active layers were all treated by SVA using THF for 10 min. Initially, the IDIC (A1):$PC_{71}BM$ (A2) weight ratio was carefully scanned, while the weight ratio of D:(A1+A2) was kept at 1:1, based on previous reported results.[21] As shown in **Figure 2** and **Table 1**, the binary OSC devices based on the DRTB-T:IDIC showed a V_{OC} of 0.99 V, a J_{SC} of 14.31 mA/cm^2 and an FF of 0.629, resulting in a PCE of 8.90%.

The binary OSC devices based on the DRTB-T:$PC_{71}BM$ achieved an inferior PCE of 6.23% due to the low J_{SC} of 9.67 mA/cm^2. Consequently, we introduced $PC_{71}BM$ as the third component into the DRTB-T:IDIC binary OSC devices and found that with the increase of the $PC_{71}BM$ content, the V_{OC} has minimal change and the J_{SC} and the FF increased. Specifically, when feeding 30% $PC_{71}BM$ as acceptors (weight ratio of D:A1:A2 was 1:0.7:0.3), the V_{OC} was 0.99 V, the J_{SC} was slightly increased to 14.75 mA/cm^2, and the FF was increased to 0.648. When the $PC_{71}BM$ content was 50%, the PCE of the devices attained the highest level of 10.48%, with the J_{SC} of 15.47 mA/cm^2 and FF of 0.677. When further increasing the $PC_{71}BM$ content to 70%, the J_{SC} value started to decrease, and the PCE also downturned, which is ascribed to the insufficient absorption. In summary, as shown in **Figures 2c** and **2d**, ternary devices with 50% $PC_{71}BM$ obtained the highest J_{SC} and FF values, which contributed to the highest PCE. It is obvious that the enhancement of the J_{SC} benefited from the complementary absorption spectra. However, the FF of the ternary devices also outperformed the binary devices, which suggests that another mechanism, such as morphology modulation by introducing the third component, played a significant role in improving the device performance.

The external quantum efficiency (EQE) curves of these devices are presented in **Figure 2b**. The integrated J_{SC} values evaluated from the EQE curves are collected in **Table 1** and were consistent with the values obtained from the *J-V* test. When introducing a small amount (30%) of $PC_{71}BM$ into the $PC_{71}BM$-based binary device, the light harvesting in the short wavelength region from 380 to 480 nm was improved. A new peak centered at 450 nm emerged in the ternary devices, which is attributed to the characteristic absorption of $PC_{71}BM$. When continuing to add $PC_{71}BM$ (A1:A2=0.5:0.5), the response intensity in the short wavelength was further enhanced. Meanwhile, in the long wavelength region beyond 600 nm, the EQE was also improved and was even higher than

that of the NFA-based binary device. A higher EQE indicates improved charge generation and extraction in the IDIC domains, which is attributed to the morphology modulation effect, arising from the introduction of a large amount of $PC_{71}BM$. However, when $PC_{71}BM$ is the dominant acceptor in the ternary devices (70% $PC_{71}BM$), the long wavelength EQE significantly decreased. This resulted in an inferior J_{SC} value of 13.72 mA/cm^2.

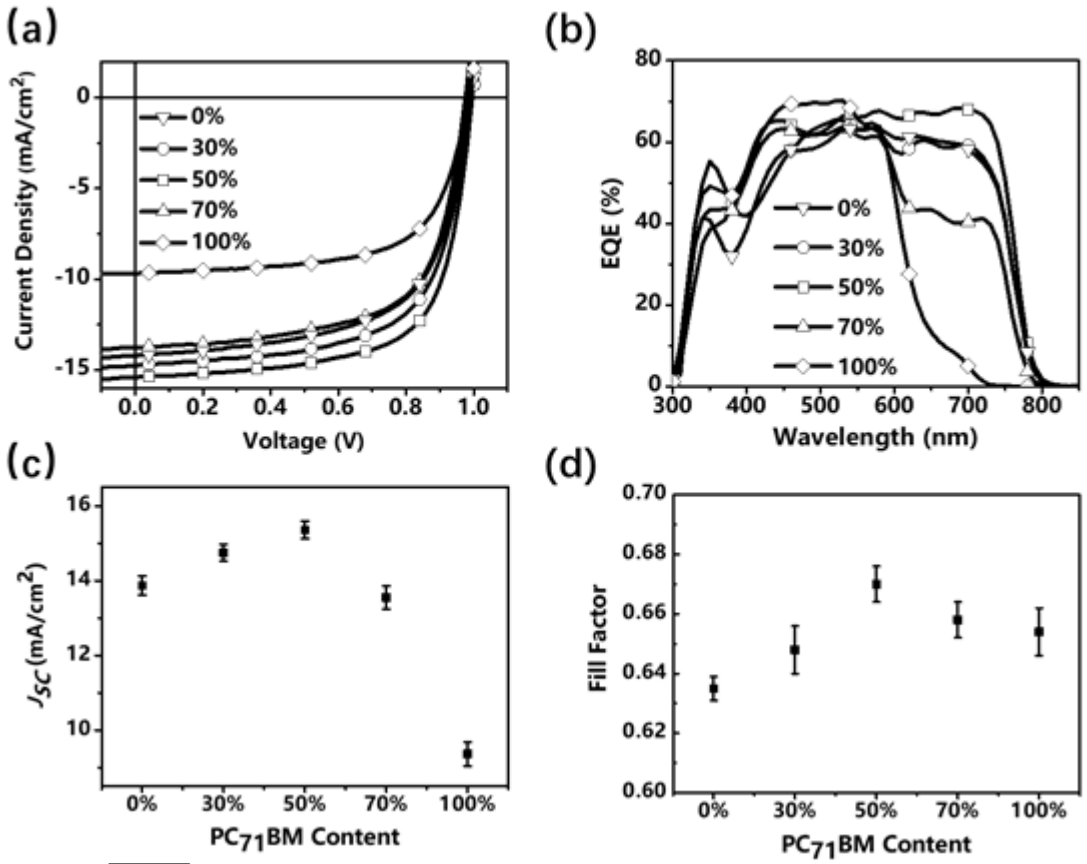

Figure 2. a) *J-V* and b) EQE curves of the OSC devices with various $PC_{71}BM$content. c) The J_{SC} and d) FF of the devices versus the weight ratio of the $PC_{71}BM$ content of the acceptors.

Table 1. The photovoltaic parameters of the OSC devices with various $PC_{71}BM$ content under AM 1.5G, 100 mW/cm^2 illumination (statistical values are shown in parentheses acquired from five different device measurements)

$PC_{71}BM$ Content	V_{OC} (V)	J_{SC} (mA/cm^2)	Integrated J_{SC} (mA/cm^2)	FF	PCE (%)
0%	0.99	14.31 (13.87±0.26)	14.01	0.629 (0.635±0.004)	8.90 (8.79±0.09)
30%	0.99	14.75 (14.75±0.22)	14.33	0.648 (0.648±0.08)	9.52 (9.42±0.06)
50%	0.99	15.47 (15.36±0.24)	15.32	0.677 (0.670±0.006)	10.48 (10.31±0.10)
70%	0.98	13.72 (13.55±0.31)	13.38	0.651 (0.658±0.006)	8.78 (8.61±0.13)
100%	0.99	9.67 (9.36±0.32)	9.25	0.653 (0.654±0.008)	6.23 (6.04±0.16)

The photocurrent analysis was performed to unearth the cause of the performance difference among the three devices (two binary devices and the champion ternary device) in light of the charge

generation and extraction processes. **Figure S2** (in Supporting Information) shows the photocurrent density (J_{ph}) versus the effective voltage (V_{eff}) characteristics for the three types of devices. As shown in the figure, all the devices revealed high charge extraction probability (P) at short-circuit conditions. For the $PC_{71}BM$-based binary devices, the NFA-based binary devices, and the ternary devices, the P values were 91%, 88% and 90%, respectively, and were evaluated by the ratio between the J_{ph} under short-circuit conditions and the saturated photocurrent (J_{sat}). Although the $PC_{71}BM$-based devices exhibited the lowest PCE and J_{SC}, their charge extraction was the most efficient among the three devices. One likely reason is that the large difference in the molecular energy levels between the $PC_{71}BM$ and the donor offered a significant driving force for exciton dissociation. By introducing $PC_{71}BM$ into the ternary devices, an energy cascade formed and facilitated the charge transfer between the donor and IDIC, which manifested as an improvement in the charge extraction possibility. Taking the high EQE values with charge extraction possibilities into account, we concluded that the electrodes in all the devices collected the charge carriers effectively once the excitons dissociated at the heterojunction. That is, in all three devices, the charge transport was smooth and recombination was weak. Hence, the primary differentiator was the charge generation (evaluated by J_{sat}) that caused the variable photovoltaic performance. which should be owed to the varied absorption spectra and the film morphology.

Furthermore, the dependency of the J_{SC} and V_{OC} on various light intensities was inspected to probe the nongeminate charge recombination dynamics of these devices.[38] The power-law dependence of the J_{SC} on the illumination intensity (P_{light}) can be expressed as $J_{SC} \propto (P_{light})^{S}$. Generally, a liner relationship between the J_{SC} and P_{light} means that the bi-molecular recombination is negligible during charge transport. For the $PC_{71}BM$-based binary devices, the NFA-based binary devices and the

ternary devices, the corresponding *S* factors were 1.0, 0.94 and 0.95, respectively, as shown in **Figure S2**. At open-circuit conditions, we also examined the relationship between the V_{OC} and P_{light} by fitting the equation of $V_{OC} \propto nk_BT/e \ln(P_{light})$, where k_B is Boltzmann's constant, T is the temperature in Kelvin, and e is the elementary charge. The fullerene devices exhibited a trap-assisted recombination characteristic with a slope of 2 k_BT/e. The other two devices, the NFA-based binary devices and the ternary devices, demonstrated a slope of 1.1 k_BT/e and 1.0 k_BT/e, respectively. This suggests that the trap-assisted recombination here was relatively minor and the bi-molecular recombination played a dominant role. In summary, the fullerene-based binary devices exhibited severe trap-assisted recombination but weak bi-molecular recombination. In the other devices containing NFA components, the bi-molecular recombination prevailed.

To unveil the performance difference caused by the film morphology, we initially used atomic force microscopy (AFM) and transmission electron microscopy (TEM) to investigate the surface and bulk morphology of the blend films. The corresponding images of the blend films treated with the THF SVA are listed in **Figure 3** and in the Supporting Information. The $PC_{71}BM$-based binary blend film showed a smooth morphology with a root mean square (RMS) surface roughness of 0.867 nm. The good miscibility between the donors and the $PC_{71}BM$ acceptors enabled the small scale, sphere-like phase separation with a domain size of *ca.* 10-20 nm (as shown in the TEM images). However, when replacing the $PC_{71}BM$ with IDIC, the lamellar domains with inerratic crystallite were achieved. The AFM images show that the DRTB-T:IDIC possessed a relatively rough surface (RMS of 5.16 nm) and strong molecular aggregation. The severe phase separation and oversized domains caused the most serious charge recombination among the three devices, as discussed previously. The ternary blend film integrated the morphological features of both the binary blends. The phase separation was still

distinct, but the domain size was modest and appropriate without the large lamellar phase. The introduction of the isotropic $PC_{71}BM$ molecules with superior compatibility alleviated the excessive crystallization and aggregation of the other two components, with an RMS of 4.16 nm.

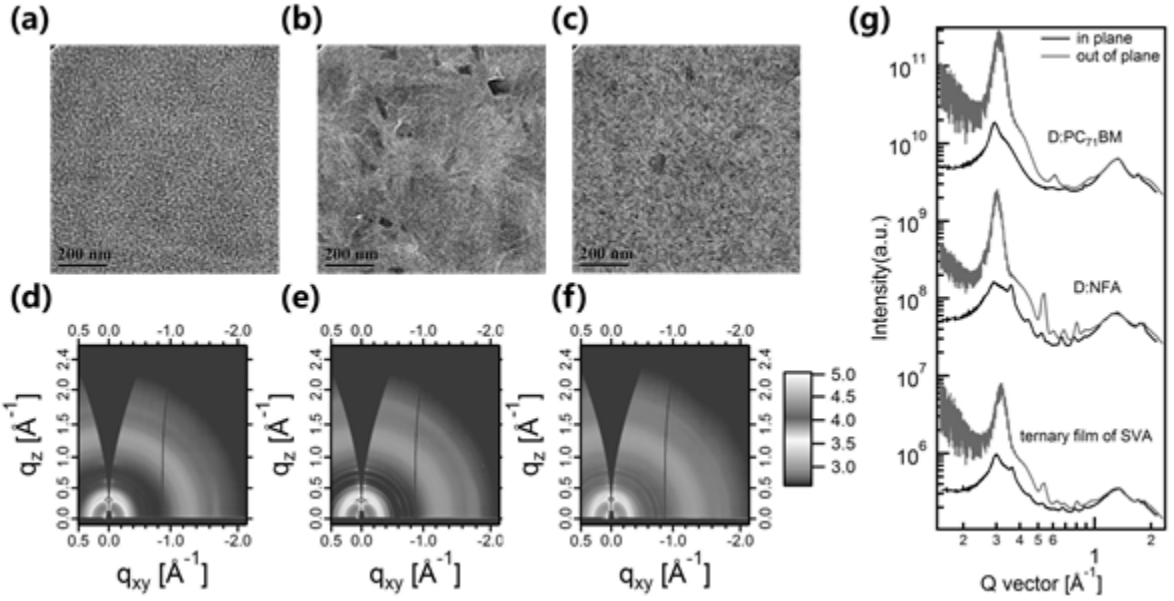

Figure 3. TEM images of (a) the fullerene-based binary blend film, (b) the NFA-based binary blend film and (c) the ternary blend film with SVA treatment. The GIWAXS 2D pattern of (d) the $PC_{71}BM$-based binary blend film, (e) the NFA-based binary blend film, and (f) the ternary blend film with SVA treatment. (g) Line profiles of the binary blend films and ternary blend film.

Since the fine crystal structure was observed in the blend films, X-ray scattering measurements were used to study the crystalline structures. We performed grazing-incidence, wide-angle X-ray scattering (GIWAXS) to correlate the crystalline behavior with the photovoltaic performance.[39, 40] The GIWAXS 2D patterns and line profiles of the two binary blend and ternary blend films were

compiled in **Figure 3**. The pristine DRTB-T film showed pronounced (100) lamellar packing peaks located at *ca.* 0.3 $Å^{-1}$ in the out-of-plane (OOP) direction with a corresponding *d*-spacing of 20.8 Å. Meanwhile, the neat IDIC exhibited (h00) lamellar peaks in the IP profile and a distinct (010) π–π stacking peak located at q = 1.8 $Å^{-1}$ in the OOP profile. The results indicate that the IDIC preferred a greater crystallization and a face-on orientation (detailed profiles of the neat donor and acceptor can be found in the Supporting Information). Comparing the NFA-based binary film with the ternary blend film with SVA, the clear lamellar (h00) peaks were similar in the in-plane direction. However, the sharp (100) peak of the ternary sample shifted from 0.30 $Å^{-1}$ to 0.32 $Å^{-1}$, indicating a more compact lamellar *d*-spacing of 19.7 Å. This suggests that introducing the $PC_{71}BM$ did not only weaken the crystallinity but also caused a denser lamellar packing.

Resonant soft X-ray scattering (RSoXS) was performed to investigate the spatial dimensions of the phase separation at different length scales and the relative domain purity.[41, 42] **Figure 4** presents the RSoXS profiles at the optimized photon energy of 284.2 eV. The NFA-based binary blends showed a distinctive phase separation with a domain size of 81.4 nm, which is consistent with the TEM images. The large domain size had a negative impact on the exciton dissociation and lowered the FF. However, the $PC_{71}BM$-based binary film exhibited a smooth and uniform morphology, giving a domain size of 15.5 nm. The introduction of $PC_{71}BM$ disturbed the strong aggregation of the NFA molecules in the ternary blend film. The domain size of the rich NFA-based phases decreased significantly to 32.9 nm, while that of the rich fullerene-based phases increased to 18.1 nm. This increase benefited the charge transport and led to a high FF. Moreover, the RSoXS also provided the relative domain purity through integration the scattering profile and calculating the total scattering intensity (TSI). Surprisingly, although the ternary devices incorporated $PC_{71}BM$, the domain purity of

the rich NFA-based phase in the ternary blend with SVA increased by 60% compared with the NFA-based binary device. This helped to suppress the charge recombination and enhance the light harvesting of the IDIC acceptors. As a result, the proper domain size and purer domains in the ternary blend film balanced the exciton dissociation and charge transport, leading to the higher J_{SC} and FF.[43]

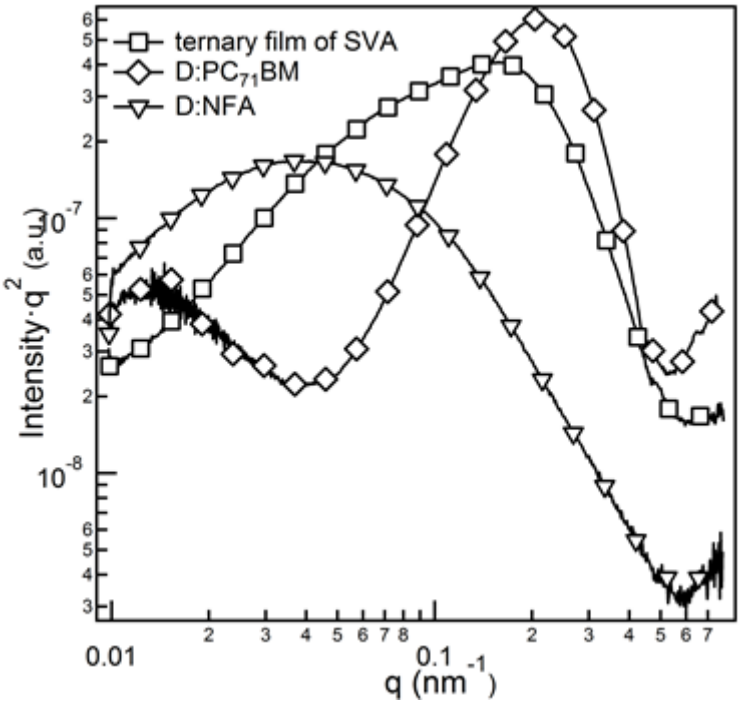

Figure 4. The RSoXS profiles of the two binary films and the ternary film with SVA.

Considering these aspects together, we can clarify the influence of the film morphology on the photovoltaic performance.[44] The $PC_{71}BM$-based binary devices exhibited the most uniform morphology and weakest crystallization, even after the SVA treatment. The poorest crystallization

had no effect on alleviating the defects or traps, which resulted in the largest trap-assisted recombination. However, the introduction of $PC_{71}BM$ with improved compatibility into the ternary devices hindered the overgrowth of crystallite, which induced more compact molecular stacking and formed smaller and purer domains. These improved domains allowed more excitons derived from the IDIC bulk to arrive at the interface and fewer charge recombinations, which accounts for the highest long wavelength EQE of the ternary devices.

In summary, the all-small-molecule ternary OSC devices consisting of two acceptors (IDIC and $PC_{71}BM$) and a donor (DRTB-T) were fabricated. The multiple components were well chosen to cover a broader absorption spectrum and form a cascade-like energy level alignment. By optimizing the component ratios and SVA treatment, a high PCE of 10.48% with improved J_{SC} and FF was achieved, which was among the best results of the reported all-small-molecule devices. The morphological characterization demonstrated that the introduction of $PC_{71}BM$ hindered the crystalline growth, alleviated the phase separation, and formed purer domains and more compact molecular stacking. The synergistic effect on the morphology and absorption of the $PC_{71}BM$ facilitated charge generation and suppressed charge recombination, which improved light harvesting and enhanced the device performance. These results correlate the domain characteristics with the device performance and offer new insight from the perspective of morphology modulation for constructing efficient ternary devices.

Supporting Information

Supporting Information is available from the Wiley Online Library or from the author.

Acknowledgements

J. Hou and C. He acknowledges the financial support of the Ministry of Science and Technology of China (2014CB643501), the National Natural Science Foundation of China (21325419, 91333204, 21604017 and 51373181), and the Chinese Academy of Sciences (XDB12030200, KJZD-EW-J01).

W.M. is thankful for support from the Ministry of Science and Technology (2016YFA0200700) and the National Natural Science Foundation of China (21504066, 21534003). The X-ray data was supported by the Director Office of Science, Office of Basic Energy Sciences, of the U.S. Department of Energy under Contract No. DE-AC02-05CH11231. The authors thank Chenhui Zhu at beamline 7.3.3, and Cheng Wang at beamline 11.0.1.2 for assistance with data acquisition.

Received: ((will be filled in by the editorial staff))
Revised: ((will be filled in by the editorial staff))
Published online: ((will be filled in by the editorial staff))

References

[1] G. Yu, J. Gao, J. C. Hummelen, F. Wudl, A. J. Heeger, *Science* **1995**, *270*, 1789.

[2] G. Li, V. Shrotriya, J. Huang, Y. Yao, T. Moriarty, K. Emery, Y. Yang, *Nat. Mater.* **2005**, *4*, 864.

[3] M. C. Scharber, D. Wuhlbacher, M. Koppe, P. Denk, C. Waldauf, A. J. Heeger, C. L. Brabec, *Adv. Mater.* **2006**, *18*, 789.

[4] B. C. Thompson, J. M. J. Fréchet, *Angew. Chem. Int. Edit.* **2008**, *47*, 58.

[5] M. Li, K. Gao, X. Wan, Q. Zhang, B. Kan, R. Xia, F. Liu, X. Yang, H. Feng, W. Ni, Y. Wang, J. Peng, H. Zhang, Z. Liang, H.-L. Yip, X. Peng, Y. Cao, Y. Chen, *Nat. Photon.* **2017**, *11*, 85.

[6] W. Zhao, S. Li, H. Yao, S. Zhang, Y. Zhang, B. Yang, J. Hou, *J. Am. Chem. Soc.* **2017**, *139*, 7148.

[7] Y. Cui, H. Yao, B. Gao, Y. Qin, S. Zhang, B. Yang, C. He, B. Xu, J. Hou, *J. Am. Chem. Soc.* **2017**, *139*, 7302.

[8] J. You, L. Dou, K. Yoshimura, T. Kato, K. Ohya, T. Moriarty, K. Emery, C.-C. Chen, J. Gao, G. Li, Y. Yang, *Nat. Commun.* **2013**, *4*, 1446.

[9] J. Y. Kim, K. Lee, N. E. Coates, D. Moses, T.-Q. Nguyen, M. Dante, A. J. Heeger, *Science* **2007**, *317*, 222.

[10] D. Baran, R. S. Ashraf, D. A. Hanifi, M. Abdelsamie, N. Gasparini, J. A. Rohr, S. Holliday, A. Wadsworth, S. Lockett, M. Neophytou, C. J. M. Emmott, J. Nelson, C. J. Brabec, A. Amassian, A. Salleo, T. Kirchartz, J. R. Durrant, I. McCulloch, *Nat. Mater.* **2017**, *16*, 363. [11] W. Zhao, S. Li, S. Zhang, X. Liu, J. Hou, *Adv. Mater.* **2017**, *29*, 1604059.

[12] R. Yu, S. Zhang, H. Yao, B. Guo, S. Li, H. Zhang, M. Zhang, J. Hou, *Adv. Mater.* **2017**, *29*, 201700437

[13] T. Liu, Y. Guo, Y. Yi, L. Huo, X. Xue, X. Sun, H. Fu, W. Xiong, D. Meng, Z. Wang, F. Liu, T. P. Russell, Y. Sun, *Adv. Mater.* **2016**, *28*, 10008.

[14] P. Cheng, C. Yan, Y. Wu, J. Wang, M. Qin, Q. An, J. Cao, L. Huo, F. Zhang, L. Ding, Y. Sun, W. Ma, X. Zhan, *Adv. Mater.* **2016**, *28*, 8021.

[15] T. Ameri, P. Khoram, J. Min, C. J. Brabec, *Adv. Mater.* **2013**, *25*, 4245.

[16] J. Zhang, Y. Zhang, J. Fang, K. Lu, Z. Wang, W. Ma, Z. Wei, *J. Am. Chem. Soc.* **2015**, *137*, 8176.

[17] G. Zhang, K. Zhang, Q. Yin, X.-F. Jiang, Z. Wang, J. Xin, W. Ma, H. Yan, F. Huang, Y. Cao, *J. Am. Chem. Soc.* **2017**, *139*, 2387.

[18] P. P. Khlyabich, B. Burkhart, B. C. Thompson, *J. Am. Chem. Soc.* **2012**, *134*, 9074.

[19] B. Fan, W. Zhong, X.-F. Jiang, Q. Yin, L. Ying, F. Huang, Y. Cao, *Adv. Energy Mater.* **2017**, *7*, 1602127.

[20] J. Zhou, Y. Zuo, X. Wan, G. Long, Q. Zhang, W. Ni, Y. Liu, Z. Li, G. He, C. Li, *J J. Am. Chem. Soc.* **2013**, *135*, 8484.

[21] L. Yang, S. Zhang, C. He, J. Zhang, H. Yao, Y. Yang, Y. Zhang, W. Zhao, J. Hou, *J. Am. Chem. Soc.* **2017**, *139*, 1958.

[22] B. Kan, M. Li, Q. Zhang, F. Liu, X. Wan, Y. Wang, W. Ni, G. Long, X. Yang, H. Feng, Y. Zuo, M. Zhang, F. Huang, Y. Cao, T. P. Russell, Y. Chen, *J. Am. Chem. Soc.* **2015**, *137*, 3886.

[23] D. Deng, Y. Zhang, J. Zhang, Z. Wang, L. Zhu, J. Fang, B. Xia, Z. Wang, K. Lu, W. Ma, Z. Wei, *Nat. Commun.* **2016**, *7*, 13740.

[24] K. Gao, W. Deng, L. Xiao, Q. Hu, Y. Kan, X. Chen, C. Wang, F. Huang, J. Peng, H. Wu, X. Peng, Y. Cao, T. P. Russell, F. Liu, *Nano Energy* **2016**, *30*, 639.

[25] H. J. Bin, Y. K. Yang, Z. G. Zhang, L. Ye, M. Ghasem, S. S. Chen, Y. D. Zhang, C. F. Zhang, C. K. Sun, L. W. Xue, C. D. Yang, H. Ade, Y. F. Li, *J. Am. Chem. Soc.* **2017**, *139*, 5085.

[26] J. Min, O. K. Kwon, C. Cui, J.-H. Park, Y. Wu, S. Y. Park, Y. Li, C. J. Brabec, *J. Mater. Chem. A* **2016**, *4*, 14234.

[27] H. Lu, J. Zhang, J. Chen, Q. Liu, X. Gong, S. Feng, X. Xu, W. Ma, Z. Bo, *Adv. Mater.* **2016**, *28*, 9559.

[28] M. Li, F. Liu, X. Wan, W. Ni, B. Kan, H. Feng, Q. Zhang, X. Yang, Y. Wang, Y. Zhang, Y. Shen, T. P. Russell, Y. Chen, *Adv. Mater.* **2015**, *27*, 6296.

[29] J. Liu, S. Chen, D. Qian, B. Gautam, G. Yang, J. Zhao, J. Bergqvist, F. Zhang, W. Ma, H. Ade, O. Inganäs, K. Gundogdu, F. Gao, H. Yan, *Nat. Energy* **2016**, *1*, 16089.

[30] H. J. Bin, L. Gao, Z. G. Zhang, Y. K. Yang, Y. D. Zhang, C. F. Zhang, S. S. Chen, L. W. Xue, C. Yang, M. Xiao, Y. F. Li, *Nat. Commun.* **2016**, *7*, 11.

[31] D. Meng, H. Fu, C. Xiao, X. Meng, T. Winands, W. Ma, W. Wei, B. Fan, L. Huo, N. L. Doltsinis, Y. Li, Y. Sun, Z. Wang, *J. Am. Chem. Soc.* **2016**, *138*, 10184.

[32] C. B. Nielsen, S. Holliday, H. Y. Chen, S. J. Cryer, I. McCulloch, *Accounts Chem. Res.* **2015**, *48*, 2803.

[33] B. Kan, H. Feng, X. Wan, F. Liu, X. Ke, Y. Wang, Y. Wang, H. Zhang, C. Li, J. Hou, Y. Chen, *J. Am. Chem. Soc.* **2017**, *139*, 4929.

[34] H. Yao, Y. Cui, R. Yu, B. Gao, H. Zhang, J. Hou, *Angew. Chem. Int. Edit.* **2017**, *129*, 3091.

[35] X. Long, Z. Ding, C. Dou, J. Zhang, J. Liu, L. Wang, *Adv. Mater.* **2016**, *28*, 6504.

[36] G. Li, Y. Yao, H. Yang, V. Shrotriya, G. Yang, Y. Yang, *Adv. Funct. Mater.* **2007**, *17*, 1636.

[37] Y. Lin, Q. He, F. Zhao, L. Huo, J. Mai, X. Lu, C.-J. Su, T. Li, J. Wang, J. Zhu, Y. Sun, C. Wang, X. Zhan, *J. Am. Chem. Soc.* **2016**, *138*, 2973.

[38] C. M. Proctor, M. Kuik, T.-Q. Nguyen, *Prog. Polym. Sci.* **2013**, *38*, 1941.

[39] H. Alexander, B. Wim, G. James, S. Eric, G. Eliot, K. Rick, M. Alastair, C. Matthew, R. Bruce, P. Howard, *J. Phys.: Conf. Ser.* **2010**, *247*, 012007.

[40] L. Zhang, W. Ma, *Chinese J. Polym. Sci.* **2017**, *35*, 184.

[41] E. Gann, A. T. Young, B. A. Collins, H. Yan, J. Nasiatka, H. A. Padmore, H. Ade, A. Hexemer, C. Wang, *Rev. Sci. Instrum.* **2012**, *83*, 045110.

[42] Y.Wu, Z. Wang, X. Meng, W. Ma. *Prog. Chem.* **2017**, *29*, 93-101.

[43] L. Ye, X. Jiao, S. Zhang, H. Yao, Y. Qin, H. Ade, J. Hou, *Adv. Energy Mater.* **2017**, *7*, 1601138.

[44] W. Ma, J. R. Tumbleston, M. Wang, E. Gann, F. Huang, H. Ade, *Adv. Energy Mater.* **2013**, *3*, 864.

An all-small-molecule ternary solar cell was achieved with a power conversion efficiency of 10.48% by incorporating the $PC_{71}BM$ into a non-fullerene small-molecule DRTB-T:IDIC binary system. The addition of $PC_{71}BM$ into DRTB-T:IDIC was found to modulate the film morphology and improved the domain purity while decreasing the domain size. This facilitated charge generation and suppressed charge recombination.

organic solar cells; non-fullerene; ternary; domain purity; small molecule

Hao Zhang, Xiaohui Wang, Liyan Yang, Shaoqing Zhang, Yun Zhang, Chang He*, Wei Ma*, Jianhui Hou.*

Improved Domain Size and Purity Enables Efficient All-Small-Molecule Ternary Solar Cells

ToC figure